Design of Mode-Locked Semiconductor Laser Comb-Based Analog Coherent Links

Elizabeth Chen, *Student Member, IEEE*, Larry A. Coldren, *Life Fellow, IEEE*, and Joseph M. Kahn, *Fellow, IEEE*

***Abstract*—Multi-wavelength analog coherent links using mode-locked laser (MLL) frequency combs as transmitter and local oscillator (LO) sources are proposed. Carrier recovery (CR) in all wavelength channels is achieved using only two optical phase-locked loops (PLLs), while polarization demultiplexing and static phase offset removal are performed using cascaded optical phase shifters. A three-section Fabry-Perot semiconductor laser structure is proposed for the comb sources. Phase-error performance in a 2.6 Tb/s system using 56-Gbaud dual-polarization quadrature phase-shift keying on 13 channels is studied. For optical and microwave beat linewidths of 2 MHz and 1 kHz, respectively, achieving phase-error penalties below 1.5 dB requires PLL delays below 400 ps. A symmetric CR scheme is shown to achieve better phase-error performance than an asymmetric CR scheme. In 13-channel analog coherent links, the MLL comb-based design is projected to consume 38% less power than a resonator-enhanced electro-optic comb-based design and 20% less power than a design using arrays of single-wavelength lasers as transmitter and LO sources, excluding modulator driver power, which is identical for the three designs.**

***Index Terms*—Carrier phase recovery, coherent detection, data center optical links, optical frequency comb, semiconductor mode-locked laser.**

I. Introduction

As DATA center links scale to higher bit rates, novel architectures that may improve density, spectral efficiency, receiver sensitivity and energy efficiency become important to study. In coherent optical links, a received signal is mixed with a strong local oscillator (LO), improving receiver sensitivity [1] and increasing link budget [2]. A coherent receiver can detect information encoded in all degrees of freedom of the signal field [3], enabling use of spectrally efficient modulation formats, such as dual-polarization (DP) phase-shift keying (PSK) or quadrature amplitude modulation.

Optical frequency combs obviate the need for multiple discrete lasers in wavelength-division-multiplexed (WDM) links. In addition, combs may simplify carrier recovery (CR) in coherent receivers [4]. Electro-optic (EO) transmitter and LO combs can be synchronized by transmitting a pilot tone to injection lock the LO seed laser, which is then used to generate an LO comb [5]. Using a pilot tone, however, leaves parts of the signal spectrum unmodulated, reducing overall spectral efficiency. Joint CR schemes using digital signal processing (DSP) exploiting phase coherence between comb lines have also been considered for comb-based links [6]. Employing high-speed DSP may, however, increase power consumption, which is not ideal for power-constrained data center systems.

Resonator-enhanced (RE) EO combs are promising candidates for coherent data center links with simplified carrier recovery. RE-EO combs fabricated on thin-film lithium niobate (TFLN) offer wide, flat spectra that may support numerous wavelength channels [7]. The phase noise of the EO comb lines is completely determined by two random variables. The seed laser phase noise is common to all comb lines, while the microwave oscillator phase noise varies linearly with the comb line index [8]. An RE-EO comb-based analog WDM coherent receiver exploits these phase noise characteristics to perform CR using only two phase-locked loops (PLLs), which control the seed laser phase noise and the the microwave oscillator phase noise, respectively [9]. A potential drawback of EO comb-based coherent transceivers is the need to integrate ultra-low-loss EO materials, such as TFLN, on silicon photonics platforms. RE-EO comb generators also suffer from inefficient conversion of seed laser power to comb output power [10]. Moreover, when a RE-EO comb is used inside a PLL, its resonator-based structure adds to the round-trip delay [9].

Semiconductor mode-locked lasers (MLLs) provide another option for comb-based links. They can be realized using III-V materials, which can be heterogeneously integrated onto silicon photonics platforms [11]. Previous work has demonstrated phase synchronization of a passively MLL to a stable reference laser on an integrated platform [12]. Two independent MLLs have been synchronized by injection locking an LO MLL to two adjacent modes of a signal MLL [13]. Coherent WDM data transmission using MLLs as both transmitter and LO has been demonstrated, using offline DSP to perform CR through a blind phase search algorithm [14].

Actively and hybridly MLLs are more stable sources than passively MLLs [15], owing to the forcing effect of microwave modulation. The modulation also provides a means for synchronizing two MLLs, similar to the synchronizaton of two EO combs [9]. This paper studies phase synchronization between hybridly MLLs generating the transmitter and LO combs in a WDM link to enable coherent detection of all the channels.

Manuscript received 19 January 2023; revised 17 April 2023; accepted 2 May 2023. Date of publication 8 May 2023; date of current version 19 September 2023. *(Corresponding author: Elizabeth Chen.)*

Elizabeth Chen and Joseph M. Kahn are with the Department of Electrical Engineering, Stanford University, Stanford 94305-9505 USA (e-mail: echen105@stanford.edu; jmk@ee.stanford.edu).

Larry A. Coldren is with the Department of Electrical and Computer Engineering, University of California Santa Barbara, Santa Barbara 93106-9560 USA (e-mail: coldren@ucsb.edu).

Color versions of one or more figures in this article are available at https://doi.org/10.1109/JLT.2023.3273479.

Digital Object Identifier 10.1109/JLT.2023.3273479

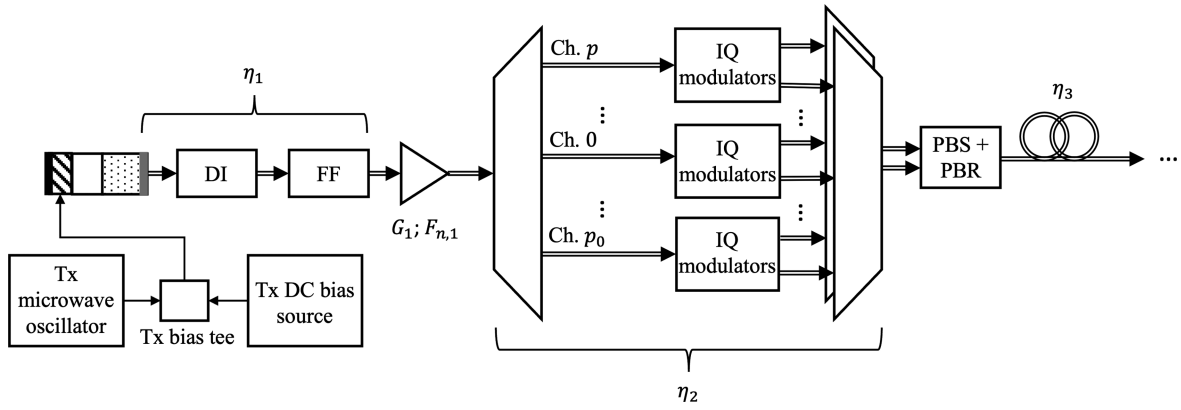

Fig. 1. MLL comb-based transmitter. A semiconductor MLL acting as a multi-wavelength source has a gain section (dotted fill), a phase-tuning section (no fill), and a saturable absorber section (striped fill). The saturable absorber section is reverse biased and modulated by a microwave source to enact hybrid mode locking. DC biases to the gain and phase-tuning sections are not shown. Tx: transmitter, DC: direct current, DI: de-interleaver, FF: flattening filter, Ch.: channel, IQ: in-phase and quadrature, PBS/R: polarization beam splitter/rotator.

All the comb lines are synchronized using just two optical PLLs, while polarization recovery is performed using cascaded phase shifters driven by marker tone detection. The proposed scheme can be implemented using analog circuitry, obviating the need for high-speed analog-to-digital converters (ADCs), which account for a significant portion of power consumption in DSP-based coherent transceivers [16], [17]. Moreover, in multi-wavelength DSP-based coherent links, the number of ADCs required scales linearly with the number of wavelength channels. The proposed analog coherent design may therefore be preferable to DSP-based designs in power-constrained links [18], [19], [20].

The comb-based architecture proposed here is similar to the RE-EO comb-based architecture proposed in [9]. This paper nevertheless makes several novel contributions:

1) it presents a hybridly MLL design based on a three-section Fabry-Perot structure appropriate for control by two PLLs in a shared CR scheme;
2) it proposes a symmetric CR configuration that achieves lower phase error between signal and LO than the asymmetric CR configuration studied in [9];
3) it draws detailed comparisons between MLL and RE-EO comb generators as sources in WDM analog coherent links, and compares these comb-based designs to those using arrays of single-wavelength lasers.

The remainder of this paper is organized as follows. Section II presents two semiconductor MLL comb-based analog coherent link designs using different CR schemes and analyzes their phase-error performance. It also presents a semiconductor MLL structure compatible with the proposed comb-based CR schemes. Section III studies an exemplary system, quantifying key performance metrics, including phase error, link SNR budget and the effect of chromatic dispersion. Section IV addresses third-order nonlinear effects on phase noise, compares MLL and RE-EO combs as sources for WDM analog coherent links, and studies the power consumption of such links using comb or single-wavelength laser sources. Section V presents conclusions.

II. Proposed Transceiver Design

In this section, we provide an overview of the proposed MLL-based analog coherent transceiver and provide a framework for analyzing the system phase-noise performance.

A. Overview

Throughout this paper, the MLL comb lines are indexed by an integer p, where $-p_0 \leq p \leq p_0$. The index $p = 0$ corresponds to the central channel, while the indices $p = \pm p_0$ correspond to the outermost channels.

Fig. 1 shows the transmitter, which uses an MLL comb as a multi-wavelength optical source. The comb may pass through a de-interleaver (DI), a flattening filter (FF), and a semiconductor optical amplifier (SOA) before data modulation. The DI ensures a sufficiently large channel spacing when the MLL comb spacing is too small to accommodate the symbol rate.

Fig. 2 shows two candidate receiver designs. Each design uses an MLL comb, nominally identical to the transmitter comb, as a multi-wavelength LO source, and uses two PLLs to perform CR for all the data-bearing channels. The two designs differ in the channels on which phase estimation is performed. The asymmetric CR design in Fig. 2(a) makes phase estimates on channels 0 and $+p_0$, while the symmetric CR design in Fig. 2(b) makes phase estimates on channels $-p_0$ and $+p_0$. In each design, the index p corresponds to any of the channels not used for phase estimation. Both designs employ optical polarization controllers based on cascaded phase shifters [18]. In each design, the two channels used for phase estimation employ type A controllers, which compensate only for polarization changes, while the other channels employ type B controllers, which compensate for polarization changes and static phase shifts [9]. Polarization varies with a timescale of several milliseconds on link lengths of tens of kilometers [21]. This variation becomes slower with shorter link lengths [22]. Polarization signal processing can therefore be driven by low-speed circuitry [18]. The phase shifters are adjusted using a marker tone detection algorithm described in [9].

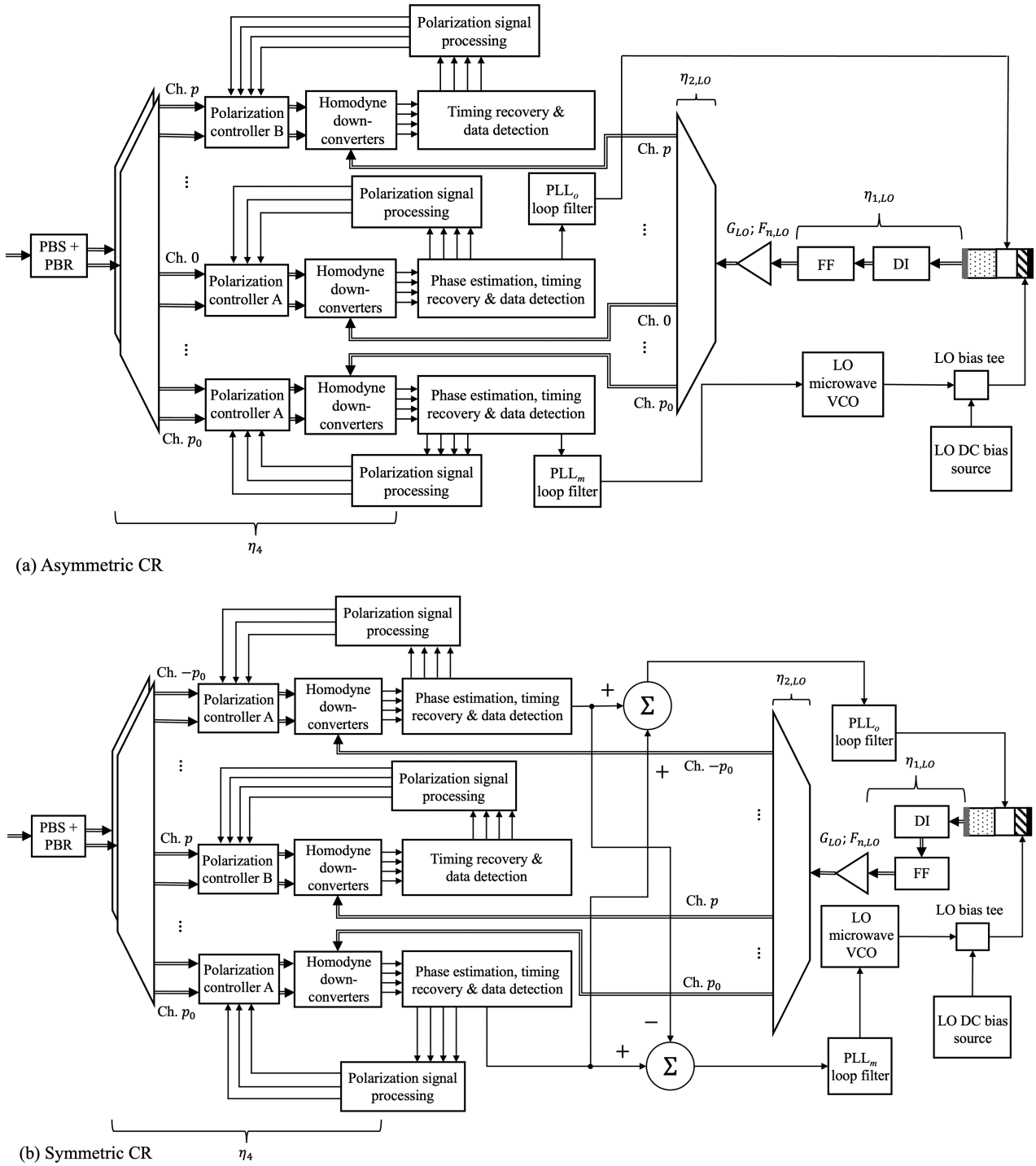

Fig. 2. Two configurations for the MLL comb-based analog coherent receiver. Each uses two PLLs to perform CR, and uses polarization controllers of type A or B to perform polarization recovery and remove static phase offsets [9]. The MLL has a gain section (dotted fill), a phase-tuning section (no fill) that determines the comb center frequency, and a microwave-modulated saturable absorber section (striped fill) that determines the comb spacing. A DC bias to the gain section is not shown. In the (a) asymmetric CR configuration, phase estimation is performed on channels 0 and p_0, and the comb line index p corresponds to any of the other channels. In the (b) symmetric CR configuration, phase estimation is performed on channels $-p_0$ and p_0, and the comb line index p corresponds to any of the other channels. PBS/R: polarization beam splitter/rotator, VCO: voltage-controlled oscillator.

The MLL design shown in Fig. 3 is proposed for the transmitter and receiver comb sources. A linear Fabry-Perot cavity has a high-reflectivity (HR) coating on one end and a low-reflectivity (LR) etched facet ($R \approx 32\%$) on the other. The cavity comprises three sections: (1) an active gain (G) section, (2) a phase-tuning (PT) section made of passive waveguide material and (3) a saturable absorber (SA) section made of reverse-biased active gain material. A microwave signal is superposed on a reverse bias to the SA section to enact hybrid mode locking [23].

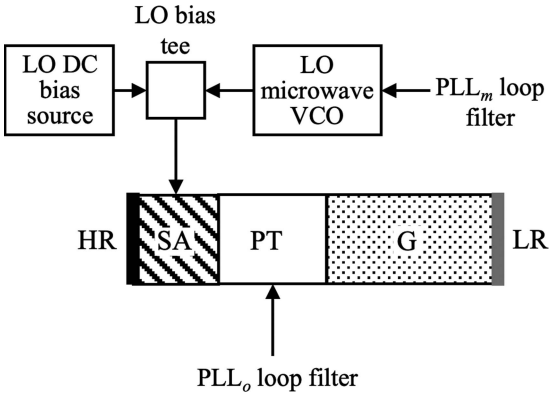

Fig. 3. Proposed MLL design (shown as used in generating the receiver LO comb). The MLL employs a three-section Fabry-Perot cavity with a high-reflectance (HR) coating and a low-reflectance (LR) etched facet ($R \approx 32\%$) on its ends. A gain (G) section comprises active gain material. A phase-tuning (PT) section comprises passive material, and receives a control current from PLL$_o$ to lock the comb center frequency f_o. A saturable absorber (SA) section comprises active gain material. It is reverse biased and modulated by a microwave voltage-controlled oscillator (VCO) to enact hybrid mode locking. The microwave VCO receives feedback from PLL$_m$ to lock the comb spacing f_m. A DC bias to the gain section is not shown.

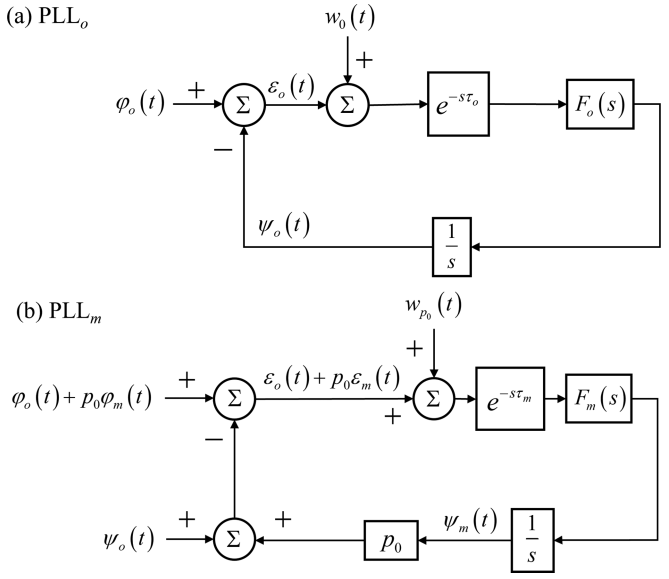

Fig. 4. Asymmetric CR receiver configuration: linearized models of (a) PLL$_o$ and (b) PLL$_m$.

The MLL output spectrum contains lines at frequencies $f_o + pf_m$ for integer values of the comb line index p. The optical frequency f_o is the frequency of the 0-th comb line, and coincides with the nominal comb center frequency. Under hybrid mode locking, the microwave modulation frequency f_m determines the comb spacing, and should coincide approximately with the cavity free spectral range (FSR).

The MLL design in Fig. 3 is designed specifically to be driven by two optical PLLs in the receiver. A first PLL, PLL$_o$, drives the PT section to control f_o, locking the common optical frequency and phase of the LO comb to those of the transmitter comb. The microwave modulation to the SA section is provided by a voltage controlled oscillator (VCO). A second PLL, PLL$_m$, drives the VCO to control f_m, locking the frequency spacings and relative phases in the LO comb lines to those in the transmitter comb.

In the following subsection, we study the phase noise of the MLL-based combs.

B. Phase Noise Analysis

The MLL in Fig. 3 has a modulated SA at one end of the cavity, similar to the device studied by Ho [24]. Ho demonstrates that under hybrid mode locking, the phase noise on the p-th comb line is given by

$$\varphi_p(t) = \sum_{n=0}^{\infty} A_n(t) H_n\left(\frac{\sqrt{2}p}{P}\right), \tag{1}$$

where P is the number of locked modes (or comb lines), and $H_n(x)$ is the n-th order Hermite polynomial. The $A_n(t)$ are expansion coefficients, which are computed by solving mode-locking equations [25] under noise perturbations. As shown by Ho, $\varphi_p(t)$ can be well-approximated by the first two terms of (1):

$$\begin{aligned}\varphi_p(t) &\approx A_0(t) + A_1(t) \cdot \frac{2\sqrt{2}p}{P} \\ &= \varphi_o(t) + p\varphi_m(t).\end{aligned} \tag{2}$$

In the second line of (2), we have defined an optical phase noise $\varphi_o(t) = A_0(t)$, which is common to all the comb lines, and a microwave phase noise $\varphi_m(t) = \frac{2\sqrt{2}}{P} A_1(t)$, whose contribution to the total phase noise (2) varies linearly with comb line index p.

The optical phase noise $\varphi_o(t)$ is a Wiener process [26], which we characterize by an optical linewidth $\Delta\nu_o$. In hybridly and passively MLLs, the microwave phase noise $\varphi_m(t)$ is also a Wiener process [27], which we characterize by a microwave linewidth $\Delta\nu_m$. The p-th comb line has a linewidth $\Delta\nu_p = \Delta\nu_o + p^2\Delta\nu_m$, which varies quadratically with comb line index p [28]. The phase noise model (2), containing a common term and a term varying linearly with comb line index, giving rise to a linewidth varying quadratically with comb line index, is consistent with other work [26], [29].

The two phase noise processes, $\varphi_o(t)$ and $\varphi_m(t)$, motivate the use of two PLLs, PLL$_o$ and PLL$_m$, in the MLL-based analog coherent receiver, as shown in Fig. 2. The PLLs in Figs. 2(a) and 2(b) can be studied using the linear models in Figs. 4 and 5, respectively.

The models employ the following notation:

1) $\varphi_o(t)$ and $\varphi_m(t)$ now denote the combined optical and microwave phases noises of the transmitter and LO combs, which are Wiener processes. $\Delta\nu_o$ and $\Delta\nu_m$ now denote the beat linewidths of these combined phase noises.
2) $\psi_o(t)$ is the optical control phase of the LO MLL, induced by the PLL$_o$ loop filter driving its PT section. $\psi_m(t)$ is the microwave control phase of the LO MLL, induced by

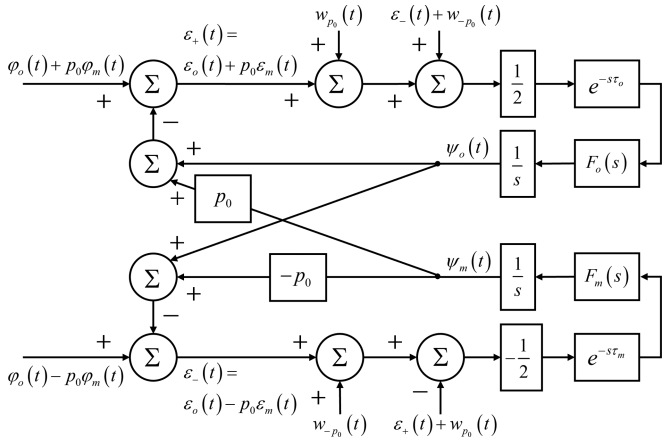

Fig. 5. Symmetric CR receiver configuration: linearized models of PLL$_o$ and PLL$_m$.

the PLL$_m$ loop filter driving the VCO modulating its SA section. The total control phase on the p-th LO comb line is $\psi_p(t) = \psi_o(t) + p\psi_m(t)$.

3) $w_i(t)$ are the additive white Gaussian noise (AWGN) components on the channels from which the PLLs derive their phase estimates. For QPSK, they have two-sided power spectral densities

$$S_{w_i w_i}(\omega) = \frac{T_s}{2\gamma_i} \qquad \text{for } i \in \{0, \pm p_0\}, \tag{3}$$

where γ_i is the symbol signal-to-noise ratio (SNR) on the i-th channel and T_s is the symbol interval [3].

4) τ_o and τ_m are the path delays of PLL$_o$ and PLL$_m$, respectively.

5) $F_o(\omega)$ and $F_m(\omega)$ are the second-order loop filter transfer functions for PLL$_o$ and PLL$_m$, respectively. They are defined as

$$F_i(\omega) = 2\zeta\omega_{n,i} + \frac{\omega_{n,i}^2}{j\omega} \qquad \text{for } i \in \{o, m\}, \tag{4}$$

where $\omega_{n,o}$ and $\omega_{n,m}$ are the natural frequencies of their associated PLLs, and $\zeta = 1/\sqrt{2}$.

6) $\varepsilon_o(t) = \varphi_o(t) - \psi_o(t)$ and $\varepsilon_m(t) = \varphi_m(t) - \psi_m(t)$ are, respectively, the optical and microwave phase errors between the transmitter and LO MLL combs. The total phase error on the p-th channel is $\varepsilon_o(t) + p\varepsilon_m(t)$.

The phase-error standard deviation on the p-th channel can be written as $\sqrt{\sigma_{\varepsilon_o}^2 + p^2\sigma_{\varepsilon_m}^2}$, where $\sigma_{\varepsilon_o}^2$ and $\sigma_{\varepsilon_m}^2$ are the variances of $\varepsilon_o(t)$ and $\varepsilon_m(t)$, respectively. Using the linear models in Figs. 4 and 5, we can find expressions for $\sigma_{\varepsilon_o}^2$ and $\sigma_{\varepsilon_m}^2$ for the asymmetric and symmetric CR configurations. Assuming all the channels used for phase estimation have the same SNR (i.e., $\gamma_0 = \gamma_{\pm p_0}$), we can express the optical phase-error variance as

$$\sigma_{\varepsilon_o}^2 = \frac{\pi\Delta\nu_o}{2\zeta\omega_{n,o}}\Gamma_o^{\text{PN}}(\omega_{n,o}\tau_o) + \frac{(1+4\zeta^2)\,\omega_{n,o}T_s}{4\zeta}\frac{1}{2n_{\text{PE}}n_c\gamma_0}\Gamma_o^{\text{AWGN}}(\omega_{n,o}\tau_o). \tag{5}$$

In (5), n_{PE} is the number of polarizations used in phase estimation [18]. We assume $n_{\text{PE}} = 2$. The variable n_c captures the difference between the two receiver CR configurations. In the asymmetric CR scheme, $n_c = 1$, while in the symmetric CR scheme, $n_c = 2$. $\Gamma_o^{\text{PN}}(\omega_n\tau)$ and $\Gamma_o^{\text{AWGN}}(\omega_n\tau)$ are given by

$$\Gamma_o^{\text{PN}}(\omega_n\tau) = \frac{2\zeta\omega_n}{\pi}\int_{-\infty}^{\infty} |j\omega + e^{-j\omega\tau}F_o(\omega)|^{-2}d\omega \tag{6}$$

$$\Gamma_o^{\text{AWGN}}(\omega_n\tau) = \frac{2\zeta}{\pi(1+4\zeta^2)\,\omega_n}\int_{-\infty}^{\infty}\left|\frac{F_o(\omega)}{j\omega + e^{-j\omega\tau}F_o(\omega)}\right|^2 d\omega \tag{7}$$

The microwave phase-error variance $\sigma_{\varepsilon_m}^2$ can likewise be found using the linear models in Figs. 4 and 5:

$$\sigma_{\varepsilon_m}^2 = \frac{\pi\Delta\nu_m}{2\zeta\omega_{n,m}}\Gamma_m^{\text{PN}}(\omega_{n,m}\tau_m) + \frac{(1+4\zeta^2)\,\omega_{n,m}T_s}{4\zeta}\frac{1}{2n_{\text{PE}}n_c\gamma_0}\Gamma_m^{\text{AWGN}}(\omega_{n,m}\tau_m) \tag{8}$$

where $\Gamma_m^{\text{PN}}(\omega_n\tau)$ and $\Gamma_m^{\text{AWGN}}(\omega_n\tau)$ are given by

$$\Gamma_m^{\text{PN}}(\omega_n\tau) = \frac{2\zeta\omega_n}{\pi}\int_{-\infty}^{\infty} |j\omega + p_0e^{-j\omega\tau}F_m(\omega)|^{-2}d\omega \tag{9}$$

$$\Gamma_m^{\text{AWGN}}(\omega_n\tau) = \frac{2\zeta}{\pi(1+4\zeta^2)\,\omega_n}\cdot \int_{-\infty}^{\infty}\left|\frac{F_m(\omega)}{j\omega + p_0e^{-j\omega\tau}F_m(\omega)}\right|^2 d\omega \tag{10}$$

In the following section, we study the performance of the MLL-based analog coherent receiver with a design example.

III. Design Example

In this section, we study a multi-wavelength system operating in the O-band, using dual-polarization quadrature phase-shift keying (DP-QPSK) at 56 GBaud symbol rate. The comb spans of integrated semiconductor MLLs are typically limited to tens of nanometers by gain bandwidth and waveguide dispersion [30]. For instance, [31] reports a span of roughly 13 nm for an InGaAsP/InP quantum well device. We conservatively assume a comb span of 1 THz (about 6 nm) and a comb spacing of 40 GHz for the transmitter and LO MLLs. Using DIs to keep only even-indexed comb lines, the system provides 13 data-modulated channels at a channel spacing of 80 GHz. The outermost channels correspond to comb line indices of $\pm p_0 = \pm 12$.

We assume a pre-forward error correction (FEC) bit-error ratio (BER) of 2.4×10^{-4}, which applies to FEC codes including RS(544, 514). Achieving the target BER requires an SNR per symbol of 10.6 dB for QPSK on an ideal AWGN channel [3]. Considering overhead, the system provides a net bit rate of 2.6 Tb/s.

A. Phase Error

To keep the SNR penalty due to phase error below 1.5 dB, the phase-error standard deviation on each channel should not

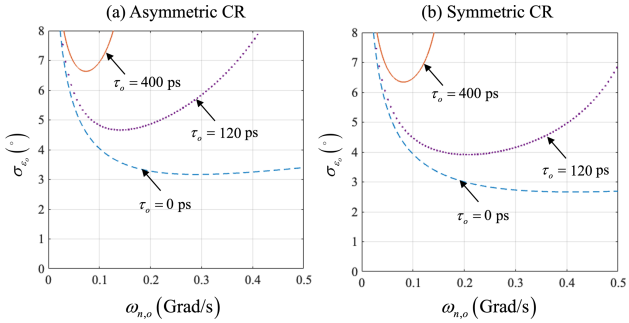

Fig. 6. Optical phase-error standard deviation σ_{ε_o} versus PLL$_o$ natural frequency $\omega_{n,o}$ at two values of the loop delay τ_o. The beat optical linewidth is $\Delta\nu_o = 2$ MHz and the SNR per symbol is $\gamma_0 = 10.6$ dB. When $\tau_o = 120$ ps, at the optimal $\omega_{n,o}$, σ_{ε_o} is 4.66° for the asymmetric CR scheme and 3.91° for the symmetric CR scheme. When $\tau_o = 400$ ps, at the optimal $\omega_{n,o}$, σ_{ε_o} is 6.62° for the asymmetric CR scheme and 6.34° for the symmetric CR scheme.

exceed 7.4° for QPSK [32]. We assume the beat optical linewidth of the transmitter and LO combs is $\Delta\nu_o = 2$ MHz. This is achievable using the linear cavity design shown in Fig. 3 [12]. Similar linewidths have been reported for InAs/InP Fabry-Perot devices [33]. The microwave linewidth of actively or hybridly MLLs can be lower than 100 Hz [34], [12]. We assume the beat microwave linewidth of the transmitter and LO combs is $\Delta\nu_m = 1$ kHz. The corresponding microwave phase noise of each comb exceeds that of a low-power monolithic VCO in a similar frequency range [35]. We consider two choices for the delays, τ_o and τ_m. The first choice, $\tau_o = \tau_m = 120$ ps, corresponds to the minimum delay achieved in a single-wavelength PLL in photonic integrated circuits (PICs) [36], and represents a lower bound for comb-based integrated PLLs. The second choice, $\tau_o = \tau_m = 400$ ps, corresponds to the maximum value for which the comb-based analog coherent receiver can achieve a phase-error penalty below 1.5 dB, as explained below.

Fig. 6 shows the optical phase-error standard deviation σ_{ε_o} against $\omega_{n,o}$, the natural frequency of PLL$_o$, for different values of the loop delay τ_o, for the asymmetric and symmetric CR designs at $\gamma_0 = 10.6$ dB. For $\tau_o = 120$ ps, at the respective optimal values of $\omega_{n,o}$, the asymmetric scheme achieves an optical phase-error standard deviation of $\sigma_{\varepsilon_o} = 4.66°$, while the symmetric scheme achieves $\sigma_{\varepsilon_o} = 3.91°$. For $\tau_o = 400$ ps, the asymmetric scheme achieves an optical phase-error standard deviation of $\sigma_{\varepsilon_o} = 6.62°$, while the symmetric scheme achieves $\sigma_{\varepsilon_o} = 6.34°$. Fig. 7 shows received DP-QPSK signal constellations in the central channel ($p = 0$) without and with CR by PLL$_o$.

Fig. 8 shows the microwave phase-error standard deviation on the p_0-th channel, $p_0\sigma_{\varepsilon_m}$, against $\omega_{n,m}$, the natural frequency of PLL$_m$, for different values of the loop delay τ_m, for the asymmetric and symmetric CR designs at $\gamma_0 = 10.6$ dB. In Fig. 8, for $\tau_m = 120$ ps, at the respective optimal values of $\omega_{n,m}$, the asymmetric scheme achieves $p_0\sigma_{\varepsilon_m} = 1.90°$, while the symmetric scheme achieves $p_0\sigma_{\varepsilon_m} = 1.41°$. For $\tau_m = 400$ ps, the asymmetric scheme achieves $p_0\sigma_{\varepsilon_m} = 2.12°$, while the symmetric scheme achieves $p_0\sigma_{\varepsilon_m} = 1.72°$.

We will choose p_0 to be an outermost channel, i.e., $|p| \leq |p_0|$ for all p. In that case, the total phase-error standard deviation on

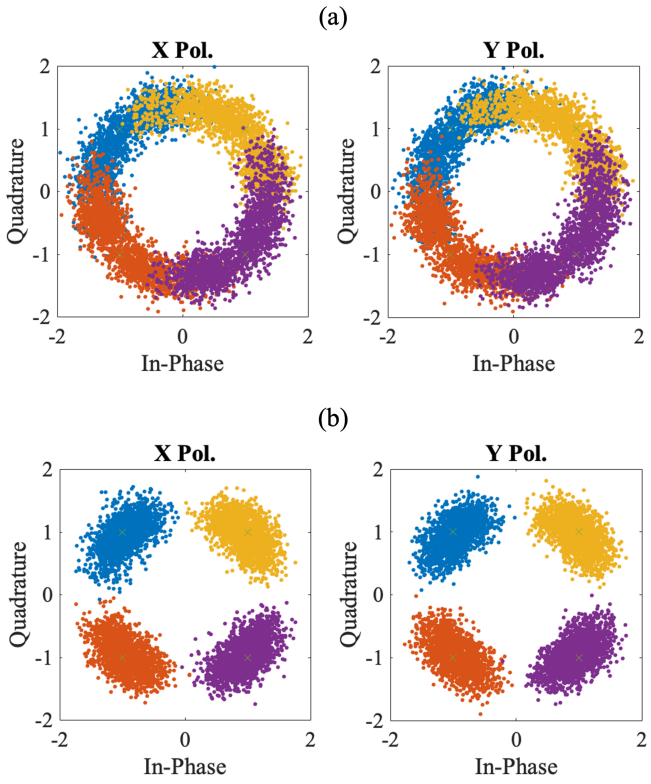

Fig. 7. Received DP-QPSK consellation diagrams in the central channel ($p = 0$) (a) without and (b) with CR by PLL$_o$, over an interval of 8192 symbol periods.

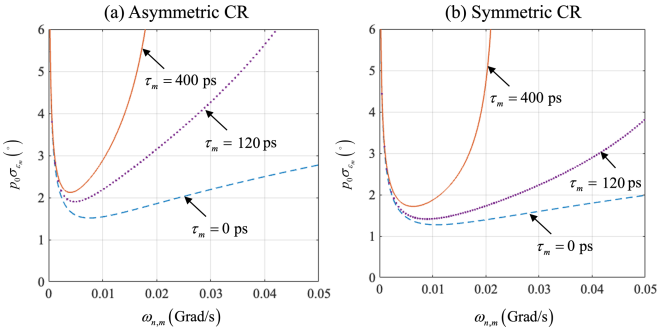

Fig. 8. Microwave phase-error standard deviation $p_0\sigma_{\varepsilon_m}$ on the p_0-th channel versus PLL$_m$ natural frequency $\omega_{n,m}$ at two values of the loop delay τ_m. The beat microwave linewidth is $\Delta\nu_m = 1$ kHz and the SNR per symbol is $\gamma_0 = 10.6$ dB. When $\tau_m = 120$ ps, at the optimal $\omega_{n,m}$, $p_0\sigma_{\varepsilon_m}$ is 1.90° for the asymmetric CR scheme and 1.41° for the symmetric CR scheme. When $\tau_m = 400$ ps, at the optimal $\omega_{n,m}$, $p_0\sigma_{\varepsilon_m}$ is 2.12° for the asymmetric CR scheme and 1.72° for the symmetric CR scheme.

the p-th channel, $\sqrt{\sigma_{\varepsilon_o}^2 + p^2\sigma_{\varepsilon_m}^2}$, will not exceed that on the p_0-th channel, which is $\sqrt{\sigma_{\varepsilon_o}^2 + p_0^2\sigma_{\varepsilon_m}^2}$. Assuming the loop delays are $\tau_o = \tau_m = 400$ ps, the total phase-error standard deviation on any channel will not exceeed 7.0° in the asymmetric receiver configuration and 6.6° in the symmetric receiver configuration. Both the asymmetric and symmetric CR schemes yield phase-error SNR penalties below 1.5 dB.

To maintain low phase-error standard deviation, both schemes require the loop delays, τ_o and τ_m, to not exceed 400 ps. Optical

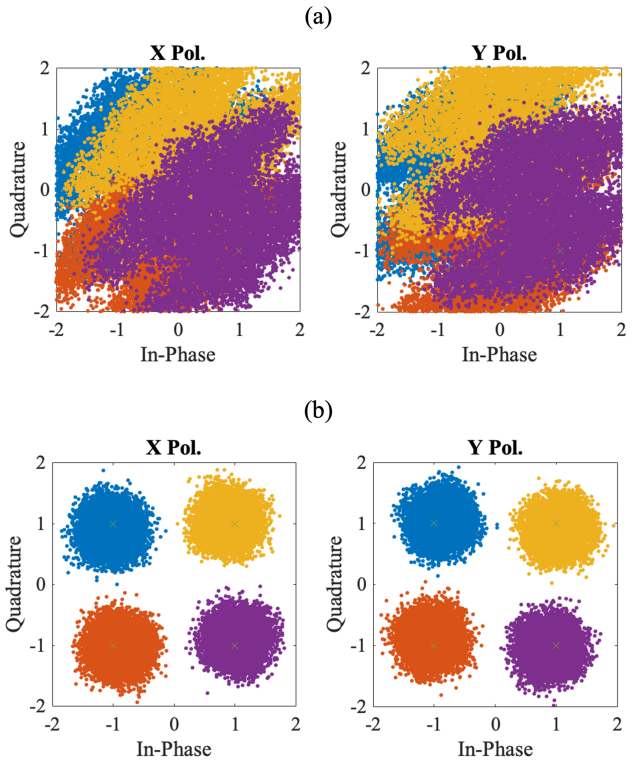

Fig. 9. Received DP-QPSK constellation diagrams (a) without and (b) with polarization recovery and phase offset removal by a type B polarization controller.

PLLs on PICs locking independent lasers have achieved loop delays as low as 120 ps [36]. The PLLs in the MLL comb-based receiver contain similar components, with the addition of an arrayed waveguide grating (AWG) for de-multiplexing the LO comb. Calculations based on optical path length suggest that compact SiN AWGs can have delays of roughly 100 ps [37]. This suggests that loop delays as small as about 220 ps are achievable with MLL comb-based systems.

As explained in Section II-A, polarization recovery and compensation of static phase offsets are achieved using phase shifter-based polarization controllers [9]. Fig. 9 shows the received DP-QPSK constellations without and with polarization control and static phase offset removal by a type B controller.

B. Chromatic Dispersion

Monte Carlo link simulations assuming 5-th order Bessel transmitter and receiver responses with bandwidths equal to 0.7 times the baud rate are performed to determine the tolerable dispersion for QPSK. For a penalty less than 1 dB with a target BER of 2.4×10^{-4}, the accumulated dispersion must be limited to $|DL| \leq 25$ ps/nm. In standard single-mode fiber with 13 channels with 80-GHz spacing centered at 1310 nm, this corresponds to a dispersion-limited transmission distance of about 100 km.

C. Signal-to-Noise Ratio

The target BER of 2.4×10^{-4} requires an SNR per symbol of 10.6 dB on an ideal AWGN channel. Allowing penalties for phase error, chromatic dispersion, polarization recovery [9] and linear crosstalk at 80-GHz channel spacing of 1.5 dB, 1.0 dB, 0.5 dB and 0.5 dB, respectively, we desire to operate at an SNR per symbol of 14.1 dB. Additive noises in the comb-based link include thermal noise, shot noise, noise arising from the LO beating with amplified spontaneous emission (ASE) on the signal, and noise arising from the signal beating with ASE on the LO [9].

TABLE I
LOSS, GAIN AND POWER VALUES FOR EXEMPLARY MLL COMB-BASED SYSTEM

Laser-to-PIC coupling loss, DI IL, and FF IL (η_1, $\eta_{1,LO}$)	5.5 dB	[38], [39]
Tx (de-)multiplexing, and DP-IQ modulation loss (η_2)	8 dB	[16], [40]
LO de-multiplexing, and downconversion loss ($\eta_{2,LO}$)	7.5 dB	[16]
Channel loss (η_3)	10 dB	[41]
Rx de-multiplexing, polarization controller, and downconversion loss (η_4)	10 dB	[16]
Booster amplifier 1 gain (G_1)	16 dB	N/A
LO booster amplifier gain (G_{LO})	14 dB	N/A
Booster amplifier noise figure ($F_{n,1}$, $F_{n,LO}$)	7 dB	[43]
Lowest Tx MLL output comb line	-2 dBm	N/A
Lowest LO MLL output comb line	0 dBm	N/A

Table I lists link parameters used to compute SNR per symbol. Values are taken from the references listed in the rightmost column of Table I. For instance, the first row assumes insertion losses (ILs) or coupling losses of 3 dB, 0.5 dB, and 2 dB for the DI, FF, and MLL-to-PIC coupling. The fourth row assumes a channel loss of 10 dB, corresponding to a fiber length of about 28 km. Link performance is limited by the channel using the comb line with the lowest power. The last two rows of Table I therefore use the lowest comb line powers of the respective combs.

The SOA gain values are picked to ensure sufficient SNR to meet the target BER. Both SOAs in the transceiver are operated in saturation. The impact of SOA saturation is discussed in Section IV-A. The values from Table I result in a worst-case SNR per symbol of 17.8 dB. The net unallocated link margin is 3.7 dB.

IV. DISCUSSION

In the first subsection below, we discuss the effects of nonlinearities induced by gain saturation in the SOAs. Then, in the next three subsections, we compare MLL and RE-EO comb-based links in terms of comb span, optical linewidth and power consumption. These comparisons refer to Table II, which summarizes high-level differences between the two comb generators. In the final subsection, we compare asymmetric and symmetric CR schemes.

A. Semiconductor Optical Amplifier Saturation

Saturated operation of an SOA causes nonlinear effects [1]. In particular, four-wave mixing (FWM) generates components at the nominal comb frequencies $\omega_o + p\omega_m$, which may include

TABLE II
COMPARISON OF MLL AND RE-EO COMBS FOR WDM ANALOG COHERENT LINKS

Comb Type	Span	Material	Optical Linewidth	Power Consumption
MLL	About 1 THz	III-V semiconductor	Hundreds of kHz to MHz	32.5 (8.6) W
RE-EO	More than 1 THz	TFLN	Follows seed laser	37.9 (14.0) W

* Power consumptions are quoted for 13-channel links at 56 GBaud using DP-QPSK modulation. Values in parentheses exclude modulator driver power consumption, which is identical for the two link designs.

$|p| > p_0$, corresponding to frequencies not present in the MLL output. The comb spectrum at the SOA output can be computed accurately using the model in [43], informing the design of the FFs shown in Fig. 2(a) and (b).

Under FWM, the model (2) for the phase noise on the p-th comb line remains valid. If comb lines at frequencies $\omega_i = \omega_o + p_i\omega_m$, $\omega_j = \omega_o + p_j\omega_j$, and $\omega_k = \omega_o + p_k\omega_m$ undergo FWM, components are generated at frequencies $\omega_{ijk+} = \omega_i + \omega_j - \omega_k = \omega_o + (p_{ijk+})\omega_m$ and $\omega_{ijk-} = \omega_i - \omega_j + \omega_k = \omega_o + (p_{ijk-})\omega_m$, where $p_{ijk+} = p_i + p_j - p_k$ and $p_{ijk-} = p_i - p_j + p_k$ are the comb line indices of the FWM-generated components. These components will have phase noises $\varphi_o(t) + (p_{ijk+})\varphi_m(t)$ and $\varphi_o(t) + (p_{ijk-})\varphi_m(t)$, respectively, matching the predictions of the phase noise model (2).

B. Comb Span

The comb span of semiconductor MLLs is limited by the active material gain bandwidth and by cavity dispersion effects. The MLL design proposed in Fig. 3 has a comb span of approximately 1 THz in the O-band [44]. The comb span could be broadened by inserting a gain-flattening filter and/or dispersion-compensating filter in the cavity [44], [45]. Inserting these devices, however, would increase the round-trip cavity loss, increasing the phase noise. The gain bandwidth might alternatively be widened by using quantum-dot or quantum-dash active materials [46].

RE-EO comb generators also have output spectra that roll off away from the central comb line, but can achieve larger comb spans up to several THz [47]. Furthermore, such devices can be designed with the resonator FSR slightly detuned from the modulation frequency defining the comb spacing, such that the output spectrum only spans the desired comb lines [48]. For example, if only 25 comb lines are desired, the resonator FSR can be chosen so the output spectrum is concentrated in lines with indices $-12 \leq p \leq 12$.

While the wider bandwidth of an RE-EO comb may accommodate more data channels than an MLL comb, with either comb type, the number of data channels may be constrained by a limited total comb output power, or by the saturation output power of the SOA amplifying the comb output [9].

C. Optical Linewidth

The optical linewidth $\Delta\nu_o$ is a key parameter governing the phase-error performance of analog coherent receivers.

Semiconductor MLL combs can achieve optical linewidths in the hundreds of kHz to MHz range [30], but the optical linewidth depends on the cavity losses and other characteristics of the MLL comb-generating structure. As observed in the previous subsection, intracavity gain flattening or dispersion compensation may widen the comb span, but the consequent increased loss is likely to broaden the optical linewidth.

The optical linewidth of an RE-EO comb is determined by the linewidth of the seed laser [8], decoupling the optical linewidth from the design of the comb-generating structure. At the transmitter, an RE-EO comb can be seeded by an external cavity laser [49] having a linewidth as narrow as required. At the receiver, the LO comb seed laser should have a sufficiently narrow linewidth, while also having a frequency modulation (FM) bandwidth sufficient to achieve low loop delay in the receiver optical PLL [9]. A two-electrode distributed-feedback laser [50], with a linewidth of hundreds of kHz and FM bandwidth of hundreds of MHz, is a good candidate to satisfy these requirements [9]. This decoupling of the optical linewidth from the comb-generating structure makes the RE-EO comb a strong candidate for scaling to higher-order modulation formats, such as 16-QAM [9].

D. Power Consumption

In this subsection, we compare the power consumption of MLL and RE-EO comb-based analog coherent links to their counterparts employing arrays of separate lasers. All three link designs support 13 channels modulated at 56 GBaud by DP-QPSK, as assumed in Section III above. The analysis assumes equal power per channel at the Tx demultiplexer outputs in all three link designs, and at the Rx demultiplexer outputs in all three link designs.

Link power consumption is divided into four categories: (1) transmitter (Tx) optics, (2) Tx electronics, (3) receiver (Rx) optics, and (4) Rx electronics. In the comb-based designs, Tx optics includes the power required for the Tx MLL or seed laser and the Tx booster SOA, Tx electronics includes power required for the comb microwave modulation and data modulator driver circuits, and Rx optics includes power required for the LO MLL or seed laser and the LO booster SOA. In all three designs, Rx electronics includes the power required for the PLLs.

The power consumptions of the three link types are summarized in Table III. Details on the power consumption of the various components are provided in Appendix. In Table III, the columns "Tx Optics Cooling" and "Rx Optics Cooling" assume electrical power not converted to optical power is dissipated locally as heat. Assuming thermoelectric cooling of optical components, the dissipated power P_d is related to the thermoelectric cooler (TEC) power consumption P_{TEC} by the TEC coefficient of performance $\eta_{TEC} = P_d/P_{TEC}$, where a value $\eta_{TEC} = 1$ is assumed. Tracking power consumption throughout the link indicates that cooling roughly doubles the overall power

TABLE III
POWER CONSUMPTION SUMMARY

Source	Tx Optics	Rx Optics	Tx Optics Cooling	Rx Optics Cooling	Tx Electronics	Rx Electronics	Total
MLL Comb	0.8	0.8	0.8	0.8	24.1 (0.2)	5.2	32.5 (8.6)
RE-EO Comb	1.1	1.4	1.1	1.4	25.9 (2.0)	7.0	37.9 (14.0)
Laser Array	0.4	0.4	0.4	0.4	23.9 (0.0)	9.1	34.6 (10.7)

* Power values are in units of W. Values in parentheses exclude modulator driver power consumption, which is identical for the three designs.

consumption of optical components, consistent with thermal management observations in data centers [51].

As observed in Table III, the power consumed by the Tx and Rx optics and cooling in the MLL comb-based link (0.8 W + 0.8 W + 0.8 W + 0.8 W = 3.2 W) is less than in the RE-EO comb-based link (1.1 W + 1.4 W + 1.1 W + 1.4 W = 5.0 W), because in the RE-EO comb generator, conversion of seed light to usable comb lines is lossy and requires a high seed laser power. Moreover, the power consumed by the Tx electronics is lower in the MLL comb-based link than in the RE-EO comb-based link, because the SA in the MLL comb requires lower microwave drive power than the phase modulator in the RE-EO comb.

The laser array-based link consumes less power in its Tx and Rx optics and cooling (0.4 W + 0.4 W + 0.4 W + 0.4 W = 1.6 W) than the MLL or RE-EO comb-based links, as seen in Table III. Separate lasers can emit at higher power per wavelength than a frequency comb [49], and power is not lost from comb generation, de-interleaving, and flattening, so the laser array-based link avoids the power consumption associated with booster SOAs. Nevertheless, the MLL comb-based link has lower total power consumption (32.5 W) than the laser array-based link (34.6 W). Excluding modulator driver power, which is identical for the three link designs, the MLL comb-based link power consumption (8.6 W) is substantially lower than that for the laser array-based link (10.7 W). The MLL comb-based link saves power by a reduction in receiver complexity enabled by the phase-coherent combs. The comb-based analog coherent receivers use only two PLLs to achieve CR for 13 channels, while the laser array-based link needs 13 PLLs. This power savings in the MLL-comb-based link more than compensates for the power consumed by comb modulation and booster SOAs. The RE-EO comb-based link consumes more total power than the other two designs, owing especially to the high comb modulation power needed.

The power consumption of the comb-based analog coherent transceiver may be further reduced by decreasing losses associated with de-interleaving and flattening, as well as coupling and insertion losses. These improvements may be enabled by future progress in semiconductor MLL and PIC technologies. Progress in low-drive-power integrated modulators [52] can decrease the power consumption of all three link designs, increasing the fractional power savings for both MLL and RE-EO comb-based links.

E. Carrier Recovery Scheme

In Section III-A, the symmetric CR scheme was shown to achieve a lower phase-error standard deviation than the asymmetric CR scheme considering the optical and microwave phase noises in (2). As explained here, the symmetric CR scheme is also more robust to phase noise contributions that vary with higher powers of p, which are predicted by the infinite summation (1) derived by Ho [24]. For example, including terms up to $n = 2$ in (1), the combined phase noise of the transmitter and LO combs on the p-th comb line has the form

$$\varphi_p(t) = \varphi_o(t) + p\varphi_m(t) + p^2\varphi_2(t), \tag{11}$$

where $\varphi_2(t)$ is a higher-order phase noise term and the optical phase noise $\varphi_o(t)$ now includes a contribution from the $n = 2$ term in (1).

We neglect the AWGN $w_i(t)$ and loop path delays τ_o and τ_m for simplicity. Although the PLL phase detectors make noiseless measurements of the phase errors, the PT section and the microwave VCO driving the SA section in the LO MLL are constrained to effect a control phase of the form $\psi_p(t) = \psi_o(t) + p\psi_m(t)$, which varies only linearly with the comb line index p. In the symmetric CR scheme, the total LO control phase on the p-th comb line will be $\psi_p(t) = (\varphi_o + p_0^2\varphi_2) + p\varphi_m$, while in the asymmetric CR scheme, the total LO control phase will be $\psi_p(t) = \varphi_o + p(\varphi_m + p_0\varphi_2)$. We find that for $p \in [-p_0, p_0]$, the maximum absolute deviation of the symmetric CR control phase from the true phase noise is $\varphi_2 p_0^2$ at $p = 0$, while the maximum absolute deviation of the asymmetric CR control phase from the true phase noise is $2\varphi_2 p_0^2$ at $p = -p_0$, which is twice that for the symmetric CR scheme.

While the symmetric CR scheme is superior to the asymmetric CR scheme in use with the MLL comb generator, it may typically not be well-suited for use with the RE-EO comb generator. In the symmetric CR scheme, the loop delay τ_o in PLL$_o$ includes any time needed for changes in injection current to be seen by the outermost comb lines with indices $p = \pm p_0$. In the MLL comb, adjustments to the PT section injection current affect the frequencies of all comb lines simultaneously. By contrast, in the RE-EO comb, the time delay in frequency shifting seed laser light to the p-th comb line scales as pT, where T is the resonator round-trip time, since the p-th comb line corresponds to light that has traveled p times around the phase-modulated resonator [9]. In the design example of [9], where $T = 20$ ps and $p_0 = 16$, the symmetric CR design would add over 300 ps to the loop delay τ_o, degrading the PLL phase-error performance.

V. CONCLUSION

Multi-wavelength analog coherent transceivers using three-section Fabry-Perot MLLs as transmitter and LO comb sources, enabling CR for all wavelengths to be achieved using two optical PLLs, have been proposed. A symmetric CR scheme outperforms an asymmetric CR scheme in tolerance to optical

TABLE IV
TX OPTICS POWER TRACKING

Element	Source	Input Optical Power	Input Electrical Power	Output Optical Power
Laser (η_{laser}=15%)	MLL Comb	0	150	23
	RE-EO Comb	0	520	78
	Laser Array	0	430	65
SOA ($G_1 = 20$ dB; η_{SOA}=15%)	MLL Comb	2.3	600	92
	RE-EO Comb	2.3	600	92
	Laser Array	N/A	N/A	N/A
Total	MLL Comb		750	
	RE-EO Comb		1100	
	Laser Array		430	

* Power values are in units of mW.

TABLE V
RX OPTICS POWER TRACKING

Element	Source	Input Optical Power	Input Electrical Power	Output Optical Power
Laser (η_{laser}=15%)	MLL Comb	0	250	37
	RE-EO Comb	0	820	120
	Laser Array	0	430	65
SOA (G_{LO}=14 dB; η_{SOA}=15%)	MLL Comb	3.7	590	92
	RE-EO Comb	3.7	590	92
	Laser Array	N/A	N/A	N/A
Total	MLL Comb		840	
	RE-EO Comb		1400	
	Laser Array		430	

* Power values are in units of mW.

and microwave phase noises, as well as possible higher-order phase noise.

MLL comb-based links have been compared to analog coherent links using RE-EO combs or arrays of single-wavelength lasers as transmitter and LO sources. The MLL comb-based design offers the lowest overall power consumption, owing to its requirement for only two PLLs and the higher efficiency of the MLL comb compared to the RE-EO comb.

MLL comb-based transceivers are promising candidates for integration in silicon photonics, exploiting rapid advances in heterogeneous integration technologies. Reduced passive optical losses and improved MLL comb flatness may further reduce power consumption. Scaling MLL comb-based links to higher channel counts and higher-order modulation formats will likely require novel solutions to increase the MLL comb span without increasing its optical linewidth.

RE-EO combs, by contrast, benefit from a decoupling of the optical linewidth from the comb-generating structure, facilitating a simultaneous scaling to higher channel counts and higher-order modulation formats. Nevertheless, the power consumption of RE-EO comb-based links is increased by requirements for high microwave modulation power and high seed laser power. Their low-cost implementation will likely require advances in integration of ultra-low-loss EO materials, such as TFLN, in silicon photonics platforms.

APPENDIX
POWER CONSUMPTION ANALYSIS

The power consumed by active optical components in the Tx and Rx in the three link designs is detailed in Tables IV and V, respectively. Each active optical element receives input optical and/or electrical power, and outputs optical power. In the rows labeled "Laser", the seed laser of the RE-EO comb has a wall-plug efficiency (WPE) of 15% [53]. The conversion of seed laser light to the central 25 comb lines has an efficiency of about 30% [48]. Power loss associated with de-interleaving, flattening, and coupling before amplification is estimated as 9.9%. This results in 2.3 mW of optical power at the Tx SOA input and 3.7 mW at the Rx SOA input for the RE-EO comb link, as indicated. The WPE of the MLL laser is estimated as 15% [30]. The power loss associated with de-interleaving, flattening, and coupling before amplification is estimated as 9.9%, similar to the RE-EO comb link. This results in 2.3 mW of optical power at the Tx SOA input and 3.7 mW at the Rx SOA input for the MLL comb link, as indicated. In the laser array-based link, the total laser output power is 65 mW at both the Tx and Rx so the power per channel at the output of the Tx and Rx demultiplexers is the same for all three link designs. The Tx and Rx SOAs are assumed similar to the device in [43], which has an estimated a WPE of 15%. Link losses used to compute the power input and output at each active optical component are consistent with values stated in Table I and used in the SNR calculation in Section III-C.

The power consumed by electrical components in the Tx and Rx in the three link designs is detailed in Tables VI and VII, respectively. In the rows labeled "Comb Modulation", the microwave power needed to phase modulate the RE-EO comb is estimated to be 2 W [47]. The microwave power needed to modulate the SA section of the MLL comb in hybrid mode locking is estimated to be 200 mW [12]. In the row labeled "Data Modulation" in Table VI, the IQ modulator is assumed to consume about 8.2 pJ/bit [54], corresponding to 23.9 W for 13 channels employing DP-QPSK modulation at 56 GBaud. The row labeled "Receiver Chip" in Table VII includes the receiver

TABLE VI
TX ELECTRONICS POWER TRACKING

Element	Source	Power Consumed	Reference
Comb Modulation	MLL Comb	0.20	[12]
	RE-EO Comb	2	[47]
	Laser Array	N/A	
Data Modulation	MLL Comb	23.9	[54]
	RE-EO Comb	23.9	
	Laser Array	23.9	
Total	MLL Comb	24.1	
	RE-EO Comb	25.9	
	Laser Array	23.9	

* Power values are in units of W.

TABLE VII
RX ELECTRONICS POWER TRACKING

Element	Source	Power Consumed	Reference
Comb Modulation	MLL Comb	0.20	[12]
	RE-EO Comb	2	[47]
	Laser Array	N/A	
Receiver Chip	MLL Comb	5.0	[20]
	RE-EO Comb	5.0	
	Laser Array	9.1	
Total	MLL Comb	5.2	
	RE-EO Comb	7.0	
	Laser Array	9.1	

* Power values are in units of W.

chain, comprising a transimpedance amplifier (TIA), a variable-gain amplifier (VGA), and an output buffer (OB), as well as the PLL circuity. Two polarizations are assumed to be used in phase estimation. The power consumption of the receiver chain is estimated to be 330 mW per channel, while that of each PLL circuit is estimated as 370 mW [55]. In comb-based links, each channel requires a receiver chain, but only two PLLs are required. This results in $(370\ \text{mW} \times 2 + 330\ \text{mW} \times 13) \approx 5.0$ W power consumption for the receiver chip, as indicated in Table VII. In laser array-based links, each channel requires a receiver chain and a PLL. This results in $(370\ \text{mW} \times 13 + 330\ \text{mW} \times 13) \approx 9.1$ W power consumption for the receiver chip.

ACKNOWLEDGMENT

The authors are grateful for helpful discussions with Prof. C. L. Schow and B. Buscaino.

REFERENCES

[1] G. P. Agrawal, *Fiber-Optic Communication Systems*, 3rd ed. Hoboken, NJ, USA: Wiley, 2002.
[2] B. Buscaino, E. Chen, J. W. Stewart, T. Pham, and J. M. Kahn, "External vs. integrated light sources for intra-data center co-packaged optical interfaces," *J. Lightw. Technol.*, vol. 39, no. 7, pp. 1984–1996, Apr. 2021.
[3] E. Ip, A. P. T. Lau, D. J. F. Barros, and J. M. Kahn, "Coherent detection in optical fiber systems," *Opt. Exp.*, vol. 16, no. 2, pp. 753–791, 2008.
[4] L. Lundberg et al., "Phase-coherent lightwave communications with frequency combs," *Nature Commun.*, vol. 11, no. 201, pp. 1–7, 2020.
[5] A. C. Bordonalli, M. J. Fice, and A. J. Seeds, "Optical injection locking to optical frequency combs for superchannel coherent detection," *Opt. Exp.*, vol. 23, no. 2, pp. 1547–1557, 2015.
[6] L. Lundberg et al., "Frequency comb-based WDM transmission systems enabling joint signal processing," *Appl. Sci.*, vol. 8, 2018, Art. no. 718.
[7] M. Zhang et al., "Broadband electro-optic frequency comb generation in a lithium niobate microring resonator," *Nature*, vol. 568, pp. 373–377, 2019.
[8] A. Ishizawa et al., "Phase-noise characteristics of a 25-GHz-spaced optical frequency comb based on a phase- and intensity-modulated laser," *Opt. Exp.*, vol. 21, no. 24, pp. 29186–29194, 2013.
[9] E. Chen, B. Buscaino, and J. M. Kahn, "Phase noise analysis of resonator-enhanced electro-optic comb-based analog coherent receivers," *J. Lightw. Technol.*, vol. 40, no. 21, pp. 7117–7128, pp. 1–13, Nov. 2022.
[10] M. Kourogi, K. Nakagawa, and M. Ohtsu, "Wide-span optical frequency comb generator for accurate optical frequency difference measurement," *IEEE J. Quantum Electron.*, vol. 29, no. 10, pp. 2693–2701, Oct. 1993.
[11] J. Juvert et al., "Integration of etched facet, electrically pumped, C-band Fabry-Perot lasers on a silicon photonic integrated circuit by transfer printing," *Opt. Exp.*, vol. 26, no. 17, pp. 21443–21454, 2018.
[12] J. S. Parker, "Integrated photonic comb generation: Applications in coherent communication and sensing," Ph.D. dissertation, University of California Santa Barbara, Santa Barbara, CA, USA, 2012.
[13] W. Lee and P. J. Delfyett, "Dual-mode injection locking of two independent modelocked semiconductor lasers," *Electron. Lett.*, vol. 40, no. 19, pp. 1182–1183, 2004.
[14] J. N. Kemal et al., "Coherent WDM transmission using quantum-dash mode-locked laser diodes as multiwavelength source and local oscillator," *Opt. Exp.*, vol. 27, no. 22, pp. 31164–31175, 2019.
[15] I. Kim and K. Y. Lau, "Frequency and timing stability of mode-locked semiconductor lasers-passive and active mode locking up to millimeter wave frequencies," *IEEE J. Quantum Electron.*, vol. 29, no. 4, pp. 1081–1090, Apr. 1993.
[16] T. Hirokawa et al., "Analog coherent detection for energy efficient intra-data center links at 200 Gbps per wavelength," *J. Lightw. Technol.*, vol. 39, no. 2, pp. 520–531, Jan. 2021.
[17] J. K. Perin, A. Shastri, and J. M. Kahn, "Data center links beyond 100 Gbit/s per wavelength," *Opt. Fiber Technol.*, vol. 44, 2018, Art. no. 69–85.
[18] J. K. Perin, A. Shastri, and J. M. Kahn, "Design of low-power DSP-Free coherent receivers for data center links," *J. Lightw. Technol.*, vol. 35, no. 21, pp. 4650–4662, Nov. 2017.
[19] M. Lu et al., "A widely-tunable integrated coherent optical receiver using a phase-locked loop," in *Proc. IEEE Photonic Soc. 24th Annu. Meeting*, 2011, pp. 769–770.
[20] H. Park et al., "40Gbit/s coherent optical receiver using a Costas loop," *Opt. Exp.*, vol. 20, no. 26, pp. B197–B203, 2012.
[21] H. Bulow et al., "Measurement of the maximum speed of PMD fluctuation in installed field fiber," in *Proc. Tech. Digest. Opt. Fiber Conf. 1999, Int. Conf. Integr. Opt. Opt. Fiber. Commun.*, 1999, pp. 83–85.
[22] K. Choutagunta and J. M. Kahn, "Dynamic channel modelling for mode-division multiplexing," *J. Lightw. Technol.*, vol. 35, no. 12, pp. 2451–2463, Jun. 2017.
[23] R. Kaiser and B. Huttl, "Monolithic 40-GHz mode-locked MQW DBR lasers for high-speed optical communication systems," *IEEE J. Sel. Topics Quantum Electron.*, vol. 13, no. 1, pp. 125–135, Jan./Feb. 2007.
[24] P. T. Ho, "Phase and amplitude fluctuations in a mode-locked laser," *IEEE J. Quantum Electron.*, vol. QE- 21, no. 11, pp. 1806–1813, Nov. 1985.
[25] O. P. McDuff and S. E. Harris, "Nonlinear theory of the internally loss-modulated laser," *IEEE J. Quantum Electron.*, vol. QE-3, no. 3, pp. 101–111, Aug. 1967.
[26] Y. Takushima, H. Sotobayashi, M. E. Grein, E. P. Ippen, and H. A. Haus, "Linewidth of mode combs of passively and actively mode-locked semiconductor laser diodes," *Proc. SPIE*, vol. 5595, pp. 213–227, 2004.
[27] L. A. Jiang, M. E. Grein, H. A. Haus, and E. P. Ippen, "Noise of mode-locked semiconductor lasers," *IEEE J. Quantum Electron.*, vol. 7, no. 2, pp. 159–167, Mar./Apr. 2001.
[28] V. Panapakkam et al., "Amplitude and phase noise of frequency combs generated by single-section InAs/InP quantum-dash-based passively and actively mode-locked lasers," *IEEE J. Quantum Electron.*, vol. 52, no. 11, Nov. 2016, Art no. 1300207.
[29] D. v. d. Linde, "Characterization of the noise in continuously operating mode-locked lasers," *Appl. Phys. B*, vol. 39, pp. 201–217, 1986.
[30] L. Chang, S. Liu, and J. E. Bowers, "Integrated optical frequency comb technologies," *Nat. Photon.*, vol. 16, pp. 95–108, 2022.
[31] M. Zander et al., "High performance BH InAs/InP QD and InGaAsP/InP QW mode-locked lasers as comb and pulse sources," in *Proc. Opt. Fiber Commun. Conf. Exhib.*, 2020, Paper T3C.4.
[32] E. Ip and J. M. Kahn, "Carrier synchronization for 3- and 4-bit-per-Symbol optical transmission," *J. Lightw. Technol.*, vol. 23, no. 12, pp. 4110–4124, Dec. 2005.
[33] Y. Mao, Z. Lu, J. Liu, P. J. Poole, and G. Liu, "Pulse timing jitter estimated from optical phase noise in mode-locked semiconductor quantum dash lasers," *J. Lightw. Technol.*, vol. 38, no. 17, pp. 4787–4793, 2020.

[34] E. Martin et al., "Terahertz-bandwidth coherence measurements of a quantum dash laser in passive and active mode-locking operation," *Opt. Lett.*, vol. 37, no. 23, pp. 4967–4969, 2012.
[35] H. Li and H. Rein, "Millimeter-wave VCOs with wide tuning range and low phase noise, fully integrated in a SiGe bipolar production technology," *IEEE J. Solid-State Circuits*, vol. 38, no. 2, pp. 184–191, Feb. 2003.
[36] M. Lu et al., "An integrated 40 Gbit/s optical costas receiver," *J. Lightw. Technol.*, vol. 31, no. 13, pp. 2244–2253, Jul. 2013.
[37] K. Shang, S. Pathak, C. Qin, and S. J. B. Yoo, "Low-loss compact silicon nitride arrayed waveguide gratings for photonic integrated circuits," *IEEE Photon. J.*, vol. 9, no. 5, Oct. 2017, Art no. 6601805.
[38] M. Oguma et al., "Compact and low-loss interleave filter employing lattice-form structure and silica-based waveguide," *J. Lightw. Technol.*, vol. 22, no. 3, pp. 895–902, Mar. 2004.
[39] A. M. Vengsarkar, P. J. Lemaire, J. B. Judkins, V. Bhatia, T. Erdogan, and J. E. Sipe, "Long-period fiber gratings as band-rejection filters," *J. Lightw. Technol.*, vol. 14, no. 1, pp. 58–65, Jan. 1996.
[40] P. Dong, L. Chen, C. Xie, L. L. Buhl, and Y. Chen, "50-Gbs silicon quadrature phase-shift keying modulator," *Opt. Exp.*, vol. 20, no. 19, pp. 22181–22186, 2012.
[41] Part 3: CSMA/CD Access Method and Physical Layer Specifications Amendment 4: Media Access Control Parameters, Physical Layers, and Management Parameters for 40 Gb/s and 100 Gb/s Operation, IEEE Standard 802.3ba-2010 (Amendment to IEEE Standard 802.3-2008), 2010.
[42] G. Giuliani and D. D'Alessandro, "Noise analysis of conventional and gain-clamped semiconductor optical amplifiers," *J. Lightw. Technol.*, vol. 18, no. 9, pp. 1256–1263, Sep. 2000.
[43] C. Antonelli, A. Mecozzi, W. Li, and L. A. Coldren, "Efficient and accurate modeling of multiwavelength propagation in SOAs: A generalized coupled-mode approach," *J. Lightw. Technol.*, vol. 34, no. 9, pp. 2188–2197, May 2016.
[44] J. S. Parker, A. Bhardwaj, P. R. A. Binetti, Y. Hung, and L. A. Coldren, "Monolithically integrated gain-flattened ring mode-locked laser for comb-line generation," *IEEE Photon. Technol. Lett.*, vol. 24, no. 2, pp. 131–133, Jan. 2012.
[45] Z. Zhang, J. C. Norman, S. Liu, A. Malik, and J. E. Bowers, "Integrated dispersion compensated mode-locked quantum dot laser," *Photon. Res.*, vol. 8, no. 9, pp. 1428–1434, 2020.
[46] E. U. Rafailov, M. A. Cataluna, and W. Sibbett, "Mode-locked quantum-dot lasers," *Nature Photon.*, vol. 1, pp. 395–401, 2007.
[47] Y. Hu et al., "High-efficiency and broadband on-chip electro-optic frequency comb generators," *Nature Photon.*, vol. 16, pp. 679–685, 2022.
[48] B. Buscaino, M. Zhang, M. Loncar, and J. M. Kahn, "Design of efficient resonator-enhanced electro-optic frequency comb generators," *J. Lightw. Technol.*, vol. 38, no. 6, pp. 1400–1413, Mar. 2020.
[49] A. Malik, J. Guo, M. A. Tran, G. Kurczveil, D. Liang, and J. E. Bowers, "Widely tunable, heterogeneously integrated quantum-dot O-band lasers on silicon," *Photon. Res.*, vol. 8, no. 10, pp. 1551–1557, 2020.
[50] K. Dridi, R. Maldonado-Basilio, A. Benhsaien, X. Zhang, and T. J. Hall, "Low-threshold and narrow linewidth two-electrode MQW laterally coupled distributed feedback lasers at 1550 nm," in *Proc. 38th Eur. Conf. Exhib. Opt. Commun.*, 2012, doi: 10.1364/ECEOC.2012.Mo.1.E.4.
[51] N. El-Sayed, I. Stefanovici, G. Amvrosiadis, A. A. Hwang, and B. Schroeder, "Temperature management in data centers: Why some (might) like it hot," in *Proc. 12th ACM SIGMETRICS/PERFORMANCE Joint Int. Conf. Meas. Model. Comput. Syst.*, 2012, pp. 163–174.
[52] M. Zhang, C. Wang, P. Kharel, D. Zhu, and M. Loncar, "Integrated lithium niobate electro-optic modulators: When performance meets scalability," *Optica*, vol. 8, no. 5, pp. 652–667, 2021.
[53] R. Jones et al., "Heterogeneously integrated InP/Silicon photonics: Fabricating fully functional transceivers," *IEEE Nanotechnol. Mag.*, vol. 13, no. 2, pp. 17–26, Apr. 2019.
[54] H. Andrade, A. Maharry, L. Valenzuela, N. Hosseinzadeh, C. Schow, and J. Buckwalter, "An 8.2-pJ/bit, 56 gb/s traveling-wave modulator driver with large reverse terminations," in *Proc. IEEE BiCMOS Compound Semicond. Integr. Circuits Technol. Symp.*, 2021, pp. 1–4.
[55] L. A. Valenzuela, Y. Xia, A. Maharry, H. Andrade, C. L. Schow, and J. F. Buckwalter, "A 50-GBaud QPSK optical receiver with a phase/frequency detector for energy-efficient intra-data center interconnects," *IEEE Open J. Solid-State Circuits Soc.*, vol. 2, pp. 50–60, 2022.

Elizabeth Chen (Student Member, IEEE) received the B.A.Sc. degree in engineering science from the University of Toronto, Toronto, ON, Canada, in 2019, and the M.S. degree in electrical engineering in 2021 from Stanford University Stanford, CA, USA, where she is working toward the Ph.D. degree in electrical engineering with Stanford University. Her research interests include optical communications, optical frequency combs, and coherent data center links.

Larry A. Coldren (Life Fellow, IEEE) received the Ph.D. degree in electrical engineering from Stanford University, Stanford, CA, USA, in 1972. After 13 years in the research area with Bell Laboratories, he joined the Department of Electrical and Computer Engineering, University of California, Santa Barbara (UCSB), Santa Barbara, CA, in 1984. He was the Co-founder of the Materials Department, in 1986. From 2009 to 2011, he was the Interim Dean of the College of Engineering. He became an Emeritus Professor in 2018 and was appointed a Research Professor that same year.

In 1991, he Co-founded Optical Concepts, later acquired as Gore Photonics, to develop novel VCSEL technology and in 1998, he co-founded Agility Communications, later acquired by JDSU (now Lumentum), to develop widely tunable integrated transmitters. At UCSB, he has worked on multiple-section widely-tunable lasers and efficient vertical-cavity surface-emitting lasers (VCSELs). His group has also developed a variety of high-performance InP-based photonic integrated circuits. He has authored or coauthored more than thousand journal and conference papers, eight book chapters, a widely-used textbook, and 63 issued patents, which have received more than 39,000 citations.

He is a Fellow of OSA, and the National Academy of Inventors as well as a member of the National Academy of Engineering. He was the recipient of the 2004 John Tyndall Award, 2009 Aron Kressel Award, 2014 David Sarnoff Award, 2015 IPRM Award, and 2017 Nick Holonyak, Jr. Award.

Joseph M. Kahn (Fellow, IEEE) received the A.B., M.A., and Ph.D. degrees in physics from the University of California, Berkeley, Berkeley, CA, USA, in 1981, 1983, and 1986, respectively. During 1987–1990, he was with AT&T Bell Laboratories. In 1989, he demonstrated the first successful synchronous (i.e., coherent) detection using semiconductor lasers, achieving record receiver sensitivity. During 1990–2003, Kahn was on the Electrical Engineering and Computer Sciences Faculty, Berkeley. He demonstrated coherent detection of QPSK in 1992. In 1999, D.-S. Shiu and Kahn published the first work on probabilistic shaping for optical communications. Between 1990 and 2000, Kahn and collaborators performed seminal work on indoor and outdoor free-space optical communications and multi-input multi-output wireless communications. In 2000, Kahn and K.-P. Ho founded StrataLight Communications, whose 40 Gb/s-per-wavelength long-haul fiber transmission systems were deployed widely by AT&T, Deutsche Telekom, and other carriers. In 2002, Ho and Kahn applied to patent the first electronic compensation of fiber Kerr nonlinearity. StrataLight was acquired by Opnext in 2009. In 2003, he became a Professor of electrical engineering with the E. L. Ginzton Laboratory, Stanford University, Stanford, CA, USA. Kahn and collaborators have extensively studied rate-adaptive coding and modulation, as well as digital signal processing for mitigating linear and nonlinear impairments in coherent systems. In 2008, E. Ip and Kahn (and G. Li independently) invented simplified digital backpropagation for compensating fiber Kerr nonlinearity and dispersion. Since 2004, Kahn and collaborators have been studied propagation, modal statistics, spatial multiplexing and imaging in multi-mode fibers, elucidating principal modes and demonstrating transmission beyond the traditional bandwidth-distance limit in 2005, deriving the statistics of coupled modal group delays and gains in 2011, and deriving resolution limits for imaging in 2013. His research interests include optical frequency comb generators, coherent data center links, rate-adaptive access networks, fiber Kerr nonlinearity mitigation, ultra-long-haul submarine links, and optimal free-space transmission through atmospheric turbulence. Kahn was the recipient of the National Science Foundation Presidential Young Investigator Award in 1991. In 2000, he became a Fellow of the IEEE.